TÜBİTAK

Turkish Journal of Physics

http://journals.tubitak.gov.tr/physics/

Research Article

Turk J Phys
(2017) 41: 463 – 468
© TÜBİTAK
doi:10.3906/fiz-1704-24

First-principles modeling of GaN/$MoSe_2$ van der Waals heterobilayer

Celal YELGEL*
Department of Materials Science and Nanotechnology, Faculty of Engineering, Recep Tayyip Erdoğan University, Rize, Turkey

Received: 22.04.2017 • **Accepted/Published Online:** 05.07.2017 • **Final Version:** 10.11.2017

Abstract: We investigate structural and electronic properties of the graphene-like gallium nitride (GaN) monolayer deposited on a $MoSe_2$ monolayer by using density functional theory with the inclusion of the nonlocal van der Waals correction. The GaN is bound weakly to the $MoSe_2$ monolayer with adsorption energy of 49 meV/atom. We find that the heterobilayer is energetically favorable with the interlayer distance of 3.302 Å indicating van der Waals (vdW) type interaction and the most stable stacking configuration is verified with different deposition sequences. The heterostructure of GaN/$MoSe_2$ is found to be indirect band gap semiconductor with gap value of 1.371 eV. Our results demonstrate the potential design of new two-dimensional nanoelectronic devices based on the vdW heterostructure.

Key words: Heterostructure, first-principles, transition metal dichalcogenides, two-dimensional materials

1. Introduction

Two-dimensional (2D) layered materials with weak van der Waals (vdW) interlayer interaction have attracted tremendous research interest after the successful isolation of graphene from graphite [1]. This is due to their remarkable properties such as tunable band gap, sensitive structural properties, and applicability in technological applications such as solar cells and electronic and optoelectronic devices [2–6]. The lack of a band gap and low affinity with the existing semiconducting circuits in graphene prevent their use in practical applications in field-effect transistors (FETs) [7]. However, graphene still has wide potential for electrodes in supercapacitance and lithium-ion batteries [8–10] and in thermal conductive layers [11] in electronic devices due to its ultrahigh thermal conductivity. Graphene also leads the progress of diverse 2D layered materials such as hexagonal boron nitride (h-BN) and transition metal dichalcogenides (e.g., MoS_2, WS_2, WSe_2, and $MoSe_2$). These materials suggest a broad range of applications, such as field-effect transistors, spintronics, thermoelectrics, and energy conversion and storage [2,12–15].

The 2D layered transition metal dichalcogenides TMX_2 (TM:Mo, W; and X:S, Se) are promising candidates in potential applications in various electronic and optoelectronic devices due to their outstanding electronic, optical, and mechanical properties [15–17]. In these materials, electronic properties depend on their thickness and the structure of the layers. TMX_2 has a sizeable band gap, which is important for designing transistors. Furthermore, when bulk TMX_2 is thinned down to a monolayer, the indirect band gap of bulk TMX_2 changes to a direct band gap nature, which is highly desirable in terms of optical properties and potential applications in nanoelectronics such as photodiodes [18], photovoltaic cells [19], and photodetectors [20]. More

*Correspondence: celal.yelgel@erdogan.edu.tr

recently low power consumption of field-effect transistors, logic circuits, and phototransistors has been achieved using MoS_2 monolayers [21–23]. The heterostructures can be designed by assembling TMX_2 monolayers with a precisely chosen stacking sequence. The ability of creating heterostructures leads to a unique opportunity to expand the 2D material family. This opportunity also provides an interesting new phenomenon for materials with tailored properties and nanodevice applications [24–26].

Gallium nitride (GaN) with hexagonal wurtzite or cubic zinc-blende structure and related III–V compound semiconductors are promising materials for optoelectronic devices, especially light-emitting diodes (LEDs). The bulk GaN structure is a direct band gap semiconductor of 3.4 eV [27]. The band gap can be tuned by suitable alloy combinations and deposition on low lattice mismatched substrates, which makes GaN an attractive material for nanodevices. Until now, in order to epitaxially grow GaN, sapphire is used as the most suitable substrate. This is due to its high thermal conductivity and low cost. Recently researchers tried a variety of materials to substitute for sapphire. The main aim is to obtain high power and high efficiency in nanodevices. Therefore, research efforts on graphene like GaN and heterostructures of GaN/graphene and GaN/TMX_2 are devoted extensively to high-performance LEDs and FETs. Moreover, a recent study indicated that graphene-like GaN (g-GaN) is thermodynamically stable and has extraordinary physical properties [28]. After that study g-GaN is used as the cocatalyst for MoS_2.

In this study, the structural and electronic properties of the $GaN/MoSe_2$ heterostructure are investigated by employing density functional theory with a recently developed vdW interaction-corrected density functional theory [29]. The thermal stability of $GaN/MoSe_2$ and the high quality of its heterostructure due to low lattice mismatches of GaN and $MoSe_2$ are successfully achieved with total energy calculation. After geometry optimization calculations, the most energetically stable configuration is obtained such that the Ga atoms of monolayer GaN are directly above the Se atoms of the $MoSe_2$ monolayer and the N atoms of GaN are directly on top of the Mo atoms of the $MoSe_2$ monolayer for the $GaN/MoSe_2$ heterostructure. The interlayer distance is found to be 3.302 Å with adsorption energy of 49 meV/atom representing the vdW type interaction between the layers. We found that the $GaN/MoSe_2$ heterostructure shows an indirect band gap with a value of 1.371 eV. The reason for the indirect band gap nature is discussed with projected density of states calculations.

2. Methods

All the calculations were performed using the plane wave self-consistent field (PWSCF) code as implemented in Quantum ESPRESSO [30]. The vdW interaction-corrected density functional (DFT/rVV10) [29] approach was adopted to describe long-range dispersive interactions for the $GaN/MoSe_2$ heterostructure. The description of electron–ion interactions was conducted using ultrasoft pseudopotentials [31]. The kinetic energy cutoff for the plane waves was set to 60 Ryd. A $36 \times 36 \times 1$ Γ-centered Monkhorst–Pack k-points mesh was used to perform integrations over the 2D Brillouin zone [32]. A vacuum layer with thickness of 15 Å was employed along the perpendicular direction to simulate individual 2D crystals in the repeated slab method. In structural optimization, the positions of all the atoms were allowed to relax until energy convergence precision, maximum residual force on atoms, and maximum displacement were less than 1×10^{-6} eV/atom, 0.03 eV $Å^{-1}$, and 5×10^{-4} Å, respectively. The electron state in the self-consistent calculations was populated using the Methfessel–Paxton scheme [33] with a smearing width of 0.05 eV.

3. Results

We first start by optimizing the lattice constants of monolayer GaN and $MoSe_2$, which are found to be 3.278 Å and 3.317 Å, respectively. The bond lengths of Ga-N atoms and Mo-Se atoms are found to be 1.893 Å and 2.541 Å, respectively. These calculated lattice constants and bond lengths have good agreement with recently reported values [28,34]. Figure 1 shows the optimized structure of monolayer GaN, monolayer $MoSe_2$, and the GaN/$MoSe_2$ heterostructure. According to lattice constants of the monolayers the lattice mismatch between them is less than 1.2%. Therefore, it is adequate to use 1 × 1 unit cells of monolayer GaN and $MoSe_2$ to create the heterostructure. The GaN/$MoSe_2$ is constructed using lattice constants of both monolayer GaN and $MoSe_2$, resulting in stretching or compressing of monolayer GaN and $MoSe_2$ at 1.2%. We also calculate the equilibrium lattice constant of the GaN/$MoSe_2$ heterostructure as 3.285 Å. We conclude that when using these lattice constants for the GaN/$MoSe_2$ heterostructure there is little effect on its electronic properties with a maximum difference of 9 meV in the band gap value. To find a thermodynamically stable configuration for the GaN/$MoSe_2$ heterostructure we consider several stacking configurations: i) the Ga atoms of monolayer GaN are above the Se atoms of $MoSe_2$, the N atoms of the GaN monolayer are on top of the Mo atoms of $MoSe_2$; ii) the N atoms of monolayer GaN are above the Se atoms of $MoSe_2$, the Ga atoms of the GaN monolayer are on top of the Mo atoms of $MoSe_2$; iii) the Ga atoms of monolayer GaN are above the Mo atoms of $MoSe_2$, the N atoms of the GaN monolayer are centered above the $MoSe_2$ hexagon; iv) the N atoms of monolayer GaN are above the Se atoms of $MoSe_2$, the Ga atoms of monolayer GaN are centered above the $MoSe_2$ hexagon; v) the N atoms of monolayer GaN are above the Mo atoms of $MoSe_2$, the Ga atoms of monolayer GaN are centered above the $MoSe_2$ hexagon; vi) the Ga atoms of monolayer GaN are above the Se atoms of $MoSe_2$, the Mo atoms of monolayer $MoSe_2$ are centered above the GaN hexagon. After geometry optimization calculations, the most stable configuration is obtained as configuration (i) with the most negative binding energy. To determine the thermal stability of GaN/$MoSe_2$ the binding energy (E_b) per unit cell is calculated using the following formula:

$$E_b = E_{GaN\,/\,MoSe_2} - E_{GaN} - E_{MoSe_2},$$

where $E_{GaN\,/\,MoSe_2}$ is the total energy of the heterostructure and E_{GaN} and E_{MoSe_2} are the total energy of the free-standing GaN and $MoSe_2$ monolayer, respectively. E_b is calculated to be 49 meV/atom for the heterostructure. This represents that the formation of the heterostructure is exothermic. Furthermore, this binding energy is more negative than that of the bilayer graphene and close to the typical vdW binding energy of ∼20 meV [35]. We estimate an interlayer distance of 3.302 Å for the GaN/$MoSe_2$ heterostructure.

Figures 2a–2c show the electronic structure of monolayer GaN, monolayer $MoSe_2$, and the GaN/$MoSe_2$ heterostructure, respectively. The calculated band gaps of monolayer GaN and $MoSe_2$ are 1.712 eV and 1.453 eV, respectively, which have good agreement with previous reported studies [28,34]. We found a 6.2% smaller band gap value for monolayer $MoSe_2$ compared with experimental band gap value of 1.550 eV reported in Ref. [36], which indicates the accuracy of the computational method used in this work. This is the well-known underestimation of band gap values by density functional theory, which is explained in detail in Ref. [37]. Furthermore, the GaN/$MoSe_2$ heterostructure is yet to be experimentally investigated; therefore, this work will be guidance for experimenters. While the $MoSe_2$ monolayer exhibits a direct band gap where the valence band maximum (VBM) and conduction band minimum (CBM) are located in the K point of its Brillouin zone, the GaN monolayer has an indirect band gap where the VBM and CBM are located at the K point and Γ point, respectively. When the GaN monolayer is deposited on $MoSe_2$ monolayer the indirect band gap nature is

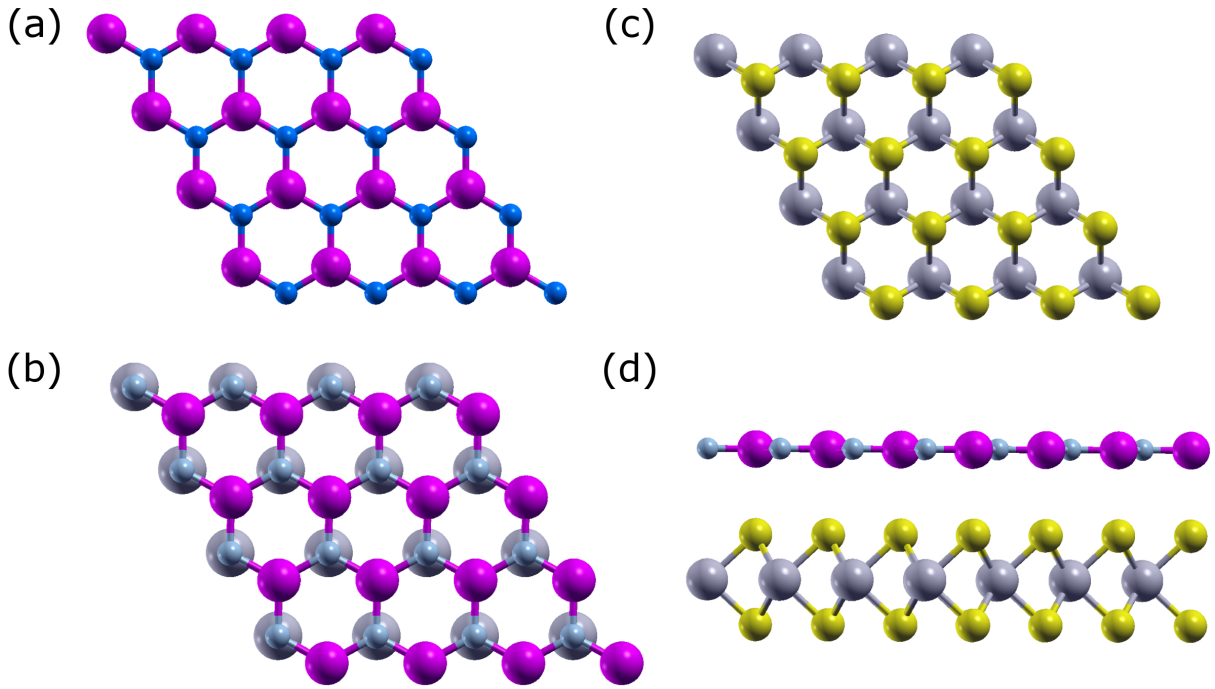

Figure 1. Atomic structures of (a) monolayer GaN, (b) monolayer $MoSe_2$, and (c, d) GaN/$MoSe_2$ heterostructure and its side view. The Ga, N, Mo, and Se atoms are represented in purple, blue, gray, and yellow, respectively.

preserved with a gap value of 1.371 eV, which is lower than that of monolayer GaN and $MoSe_2$. We also notice that there is a change in the location of the CBM, which moved 0.068 nm^{-1} from the Γ point to between the Γ point and K point.

In order to further investigate the electronic structure and describe interlayer interactions between monolayer GaN and $MoSe_2$, the total density of states (TDOS) and projected density of states (PDOS) for the GaN/$MoSe_2$ heterostructure are presented in Figure 3. The states of GaN/$MoSe_2$ around the Fermi level are mostly formed by Mo d, Se p, and N p orbitals. The CBM of the GaN/$MoSe_2$ heterostructure is contributed primarily by d and p orbitals from Mo and N atoms, respectively, while the main contribution comes from d orbitals of Mo atoms for its VBM. In the unoccupied region, there is no contribution from the GaN monolayer, whereas p orbitals of N atoms are significantly contributed to the VBM. The overlapping of electronic states between Mo d, Se p, and N p orbitals is noticed in the occupied region around E_f - 2.5 eV.

4. Conclusion

In summary, the structural and electronic properties of GaN/$MoSe_2$ heterostructures with vdW correction are studied using density functional theory. The deposition of GaN on a $MoSe_2$ monolayer is found to be exothermic, which suggests that the GaN can be grown using the $MoSe_2$ monolayer as a substrate. We found good agreement with experimental and previous calculation data for the band gap of $MoSe_2$ and GaN monolayers. Our results show that an indirect band gap of 1.371 eV is obtained when the GaN monolayer is adsorbed on the $MoSe_2$ monolayer. The effect of weak interactions between the layers on the electronic structure was investigated. The indirect band gap in the GaN monolayer is preserved with a reduction of 0.341 eV when stacking GaN on a $MoSe_2$ monolayer. We believe that these findings give insights for the development of novel 2D structures and are useful for applications in optoelectronics and in FET devices.

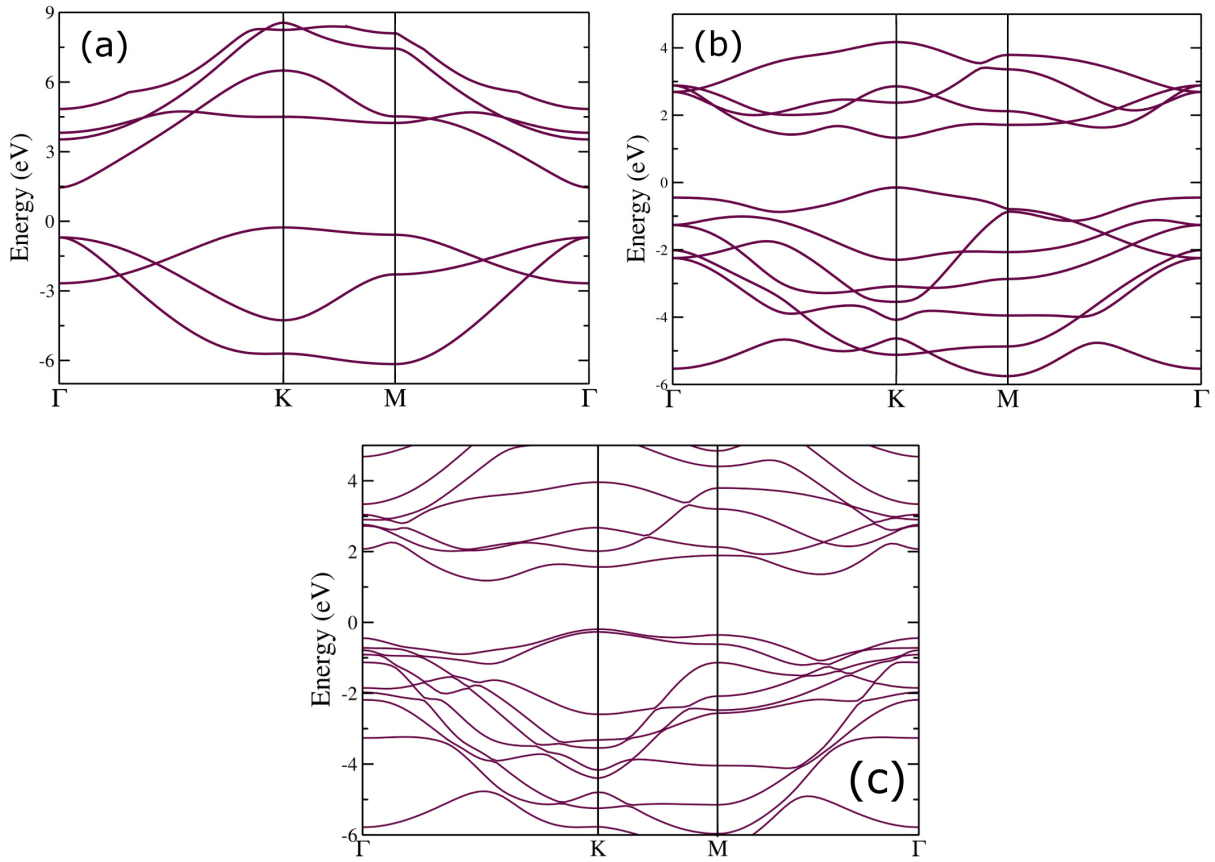

Figure 2. Electronic structures of (a) GaN monolayer, (b) $MoSe_2$ monolayer, and (c) GaN/$MoSe_2$ heterostructure. The Fermi level is set to zero.

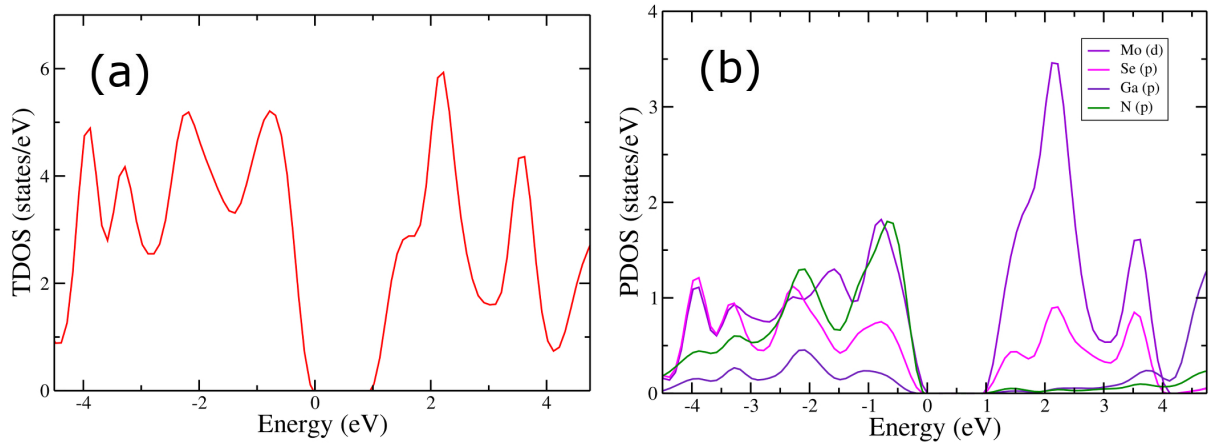

Figure 3. The TDOS and PDOS of ((a) and (b)) GaN/$MoSe_2$ heterostructure. The Fermi level is set to zero.

References

[1] Novoselov, K. S.; Geim, A. K.; Morozov, S. V.; Jiang, D.; Zhang, Y.; Dubonos, S. V.; Grigorieva, I. V.; Firsov, A. A. *Science* **2004**, *306*, 666-669.

[2] Miro, P.; Audiffred, M.; Heine, T. *Chem. Soc. Rev.* **2014**, *43*, 6537-6554.

[3] Xu, M.; Liang, T.; Shi, M.; Chen, H. *Chem. Rev.* **2013**, *113*, 3766-3798.

[4] Li, L.; Yu, Y.; Ye, G. J.; Ge, Q.; Ou, X.; Wu, H.; Feng, D. *Nat. Nanotechnol.* **2014**, *9*, 1-17.

[5] Qiao, J.; Kong, X.; Hu, Z. X.; Yang, F.; Ji, W. *Nat. Commun.* **2014**, *5*, 4475.

[6] Zhang, S.; Yan, Z.; Li, Y.; Chen, Z.; Zeng, H. *Angew. Chemie* **2015**, *127*, 3155-3158.

[7] Neto, A. H. C.; Geim, A. K. *Rev. Mod. Phys.* **2009**, *81*, 109.

[8] Luo, B.; Zhi, L. *Energy Environ. Sci.* **2015**, *8*, 456-477.

[9] Chaohe, X.; Binghui, X.; Yi, G.; Zhigang, X.; Jing, S.; Zhao, X. S. *Energy Environ. Sci.* **2013**, *6*, 1388-1414.

[10] Raccichini, R.; Varzi, A.; Passerini, S.; Scrosati, B. *Nat. Mater.* **2015**, *14*, 271-279.

[11] Shahil, K. M. F.; Balandin, A. A. *Solid State Commun.* **2012**, *152*, 1331-1340.

[12] Butler, S. Z.; Hollen, S. M.; Cao, L.; Cui, Y.; Gupta, J. A.; Gutirrez, H. R.; Heinz, T. F.; Hong, S. S.; Huang, J.; Ismach, A. F. et al. *S Nano* **2013**, *7*, 2898-2926.

[13] Rao, C. N. R.; Ramakrishna Matte, H. S. S.; Maitra, U. *Angew. Chemie Int. Ed.* **2013**, *52*, 13162-13185.

[14] Tang, Q.; Zhou, Z. *Prog. Mater. Sci.* **2013**, *58*, 1244-1315.

[15] Chhowalla, M.; Shin, H. S.; Eda, G.; Li, L. J.; Loh, K. P.; Zhang, H. *Nat. Chem.* **2013**, *5*, 263-275.

[16] Jariwala, D.; Sangwan, V. K.; Lauhon, L. J.; Marks, T. J.; Hersam, M. C. *ACS Nano* **2014**, *8*, 1102-1120.

[17] Wang, Q. H.; Kalantar-Zadeh, K.; Kis, A.; Coleman, J. N.; Strano, M. S. *Nat. Nanotechnol.* **2012**, *7*, 699-712.

[18] Baugher, B. W. H.; Churchill, H. O. H.; Yang, Y.; Jarillo-Herrero, P. *Nat. Nanotechnol.* **2014**, *9*, 262-267.

[19] Pospischil, A.; Furchi, M. M.; Mueller, T. *Nat. Nanotechnol.* **2014**, *9*, 257-261.

[20] Lopez-Sanchez, O.; Lembke, D.; Kayci, M.; Radenovic, A.; Kis, A. *Nat. Nanotechnol.* **2013**, *8*, 497-501.

[21] Radisavljevic, B; Radenovic, A; Brivio, J; Giacometti, V; Kis, A; Radisavljevic, B.; Radenovic, A.; Brivio, J.; Giacometti, V.; Kis, A. *Nat. Nano* **2011**, *6*, 147-150.

[22] Radisavljevic, B.; Whitwick, M. B.; Kis, A. *ACS Nano* **2013**, *7*, 3729.

[23] Yin, Z.; Li, H.; Li, H.; Jiang, L.; Shi, Y.; Sun, Y.; Lu, G.; Zhang, Q.; Chen, X.; Zhang, H. *ACS Nano* **2012**, *6*, 74-80.

[24] Li, H.; Shi, Y.; Chiu, M. H.; Li, L. J. *Nano Energy* **2015**, *18*, 293-305.

[25] Duan, X.; Wang, C.; Pan, A.; Yu, R.; Duan, X. *Chem. Soc. Rev.* **2015**, *44*, 8859-8876.

[26] Peng, B.; Ang, P. K.; Loh, K. P. *Nano Today* **2015**, *10*, 128-137.

[27] Moram, M. A.; Vickers, M. E. *Reports Prog. Phys.* **2009**, *72*, 36502.

[28] Zhuang, H. L.; Singh, A. K.; Hennig, R. G. *Phys. Rev. B* **2013**, *87*, 165415.

[29] Sabatini, R.; Gorni, T.; de Gironcoli, S. *Phys. Rev. B* **2013**, *87*, 41108.

[30] Giannozzi, P.; Baroni, S.; Bonini, N.; Calandra, M.; Car, R.; Cavazzoni, C.; Ceresoli, D.; Chiarotti, G. L.; Cococcioni, M.; Dabo, I. et al. *J. Phys. Condens. Matter* **2009**, *21*, 395502.

[31] Vanderbilt, D. *Phys. Rev. B* **1990**, *41*, 7892-7895.

[32] Monkhorst, H. J.; Pack, J. D. *Phys. Rev. B* **1978**, *13*, 5897-5899.

[33] Methfessel, M.; Paxton, T. *Phys. Rev. B* **1989**, *40*, 3616.

[34] Kang, J.; Tongay, S.; Zhou, J.; Li, J.; Wu, J. *Appl. Phys. Lett.* **2013**, *102*, 012111.

[35] Björkman, T.; Gulans, A.; Krasheninnikov, A. V.; Nieminen, R. M. *Phys. Rev. Lett.* **2012**, *108*, 235502.

[36] Tongay, S.; Zhou, J.; Ataca, C.; Lo, K.; Matthews, T. S.; Li, J.; Grossman, J. C.; Wu, J. *Nano Lett.* **2012**, *12*, 5576-5580.

[37] Crowley, J. M.; Tahir-Kheli, J.; Goddard, W. A. R. *J. Phys. Chem. Lett.* **2016**, *7*, 1198-1203.